R. & M. No. 3435

MINISTRY OF AVIATION

AERONAUTICAL RESEARCH COUNCIL
REPORTS AND MEMORANDA

Measurements of the Direct Pitching-Moment Derivatives for Four Wing Planforms at Transonic Speeds

By J. B. BRATT, B.A., B.Sc., W. G. RAYMER, B.Sc.(Eng.) and J. E. G. TOWNSEND
of the Aerodynamics Division, N.P.L.

LONDON: HER MAJESTY'S STATIONERY OFFICE
1966
PRICE 11*s.* 6*d.* NET

Measurements of the Direct Pitching-Moment Derivatives for Four Wing Planforms at Transonic Speeds

By J. B. BRATT, B.A., B.Sc., W. G. RAYMER, B.Sc.(Eng.) and J. E. G. TOWNSEND

of the Aerodynamics Division, N.P.L.

*Reports and Memoranda No. 3435**

December, 1952

Summary.

Measurements of the direct pitching-moment derivatives m_θ and $m_{\dot{\theta}}$ at transonic speeds for two delta and two swept wing planforms are discussed. The tests were made in the N.P.L. 9½ in. high-speed wind tunnel using slotted liners, a Mach number range from $M = 0{\cdot}695$ to $M = 1{\cdot}07$ being attained. These measurements extend earlier subsonic results obtained with solid tunnel liners into the transonic range.

Comparison with theory is made for one of the delta wings and the effect of a body on the other was examined.

1. *Introduction.*

The measurements of the direct pitching-moment derivatives m_θ and $m_{\dot{\theta}}$ described in the present paper were made in the N.P.L. 9½ in. high-speed tunnel using self-excitation apparatus[1], and they extend earlier subsonic results[2] obtained in the same tunnel into the transonic speed range. Previous measurements in this tunnel using solid liners were limited by tunnel choking to a top Mach number of about $M = 0{\cdot}95$. This upper limit has been extended to $M = 1{\cdot}07$ by means of slotted liners.

The planforms tested were two deltas (Wings A and Ā) and two swept wings (Wings B and C), the Mach number range being from $M = 0{\cdot}695$ to $M = 1{\cdot}07$. Each model was tested for one axis position, and Wings A and B† at mean incidences of 0°, 3° and 5°. Wings Ā and C were tested at 0° and 3° mean incidence.

Amplitudes of oscillation below 2° were avoided in view of results obtained during the earlier subsonic tests[2], which indicated that measurements were sensitive to random oscillatory fluctuations of flow direction in the main stream at small amplitudes and frequencies, especially in the case of models with a swept trailing edge and an axis forward of the aerodynamic centre.

The frequency parameter ω ranged from 0·042 to 0·096, and the Reynolds number from $0{\cdot}79 \times 10^6$ to $0{\cdot}96 \times 10^6$.

Wing Ā was also tested at 0° incidence with a body attached.

---

* Replaces A.R.C. 15 206 and 15 486.

† The mean incidence of Wing B varied from 2·9° to 3·0° for a nominal setting of 3·0°, and from 4·8° to 5·0° for a setting of 5·0° due to aerodynamic loading.

2. *Details of Slotted Liners.*

The tunnel walls parallel to the model axis are formed by removeable liners, which for the present tests were constructed as shown in Fig. 1. These walls were designed on the basis of tests by Holder, North and Chinneck[3]. The slots were 3/32 in. wide and were formed between $\frac{1}{2}$ in. longitudinal wooden T-section members, fixed to a wooden block at the upstream end and supported by metal combs at the downstream end. Wooden stiffening members were provided at two intermediate points, also arranged in the form of combs in order to avoid impeding the flow. The ratio of open area to total area on each liner was 0·158, and the plenum chambers beneath the walls were 2·6 in. deep.

Allowance for growth of the boundary layer was made by setting the liners to form a slightly expanding working section, the best adjustment corresponding to the smallest variation in wall pressure along the working section in the neighbourhood of the model. The tunnel walls perpendicular to the model axis were parallel and solid.

Traverses in the empty tunnel giving the variation in Mach number along the tunnel axis and along a line through the intersection of the tunnel and model axes and perpendicular to both are shown in Figs. 2a and b respectively. No attempt has been made to estimate blockage corrections for the tests with the models in the tunnel, since there is as yet no theoretical treatment which may be readily applied, even for the static case.

Mach number was measured by reference to a static-pressure hole upstream of the model at a point where the wall pressure variation along the working section remained sensibly zero over the whole Mach number range.

3. *Details of Models.*

The models were constructed of solid steel, and each represented half of a complete wing without body, the leading and trailing edges being produced to meet the aircraft centre line. A detachable body for Wing $\bar{A}$ was made of Tufnol and represented half of the aircraft body. The models are illustrated to full scale in Figs. 3 to 6. The data below relate to a complete wing.

	Wing A	*Wing B*	*Wing $\bar{A}$*	*Wing C*
Apex angle	90°	60°	80·20°	92·46°
Sweepback (L.E.)	45°	60°	49·90°	43·77°
Sweepback (T.E.)	0°	52°	3·55°	25·74°
Aspect ratio	3·00	2·88	2·97	4·42
Taper ratio	0·143	—	0·117	0·311
Root chord	4·000 in.	3·630 in.	4·500 in.	3·453 in.
Tip chord	0·572 in.	—	0·526 in.	1·074 in.
Mean chord	2·286 in.	2·356 in.	2·491 in.	2·264 in.
Span	6·856 in.	6·786 in.	6·956 in.	10·000 in.
Thickness/chord ratio	10%	6%—7%	10% (away from root)	10%
Section	RAE102	—	—	EQ1040
Axis position (distance behind apex)	$0·556c_0$	$0·689c_0$	$0·500c_0$	$0·809c_0$
Distance of A.C. behind apex	$0·534c_0$ (low speed)	$0·865c_0$ (low speed)	$0·565c_0$ ($M = 0·87$)	$0·792c_0$ ($M = 0·70$)

4. *Experimental Results.*

4.1. *Wings A and B.*

Curves relating $-m_{\dot{\theta}}$ and $-m_{\theta}$ to M are given in Figs. 7 to 12. The variation of ω with M is shown in Figs. 7 and 8 for the two test frequencies. Those curves apply to both models and all mean incidences and amplitudes to within 1%.

Mean curves for $-m_{\dot{\theta}}$ and $-m_{\theta}$ obtained with solid liners in the earlier subsonic tests[2] are included in the figures. These curves have a similar shape to those obtained with the slotted liners, differences in magnitude being attributed to the altered blockage effects and tunnel wall interference. In some instances the extension of the Mach number range up to $M = 1{\cdot}07$ brings to light changes in trend not indicated by the solid-liner tests.

The distinguishing feature of the damping derivative curves $(-m_{\dot{\theta}})$ for Wing A is the rise to a maximum in the neighbourhood of $M = 0{\cdot}95$ followed by a rapid falling-off, which in the case of the tests at incidence leads to negative damping at the lower frequency. Recovery to positive damping at higher values of M is indicated by Fig. 9. The peak value of the damping is considerably greater at a mean incidence of 5° than at 3° and 0°, and it occurs at a higher Mach number in the case of 0°. The effect of increasing frequency is to reduce the rate at which the damping falls off above the maximum in the tests at incidence.

In comparison the damping curves for Wing B show little variation over the whole Mach number range, apart from relatively small fluctuations at the upper end. The greatest tendency for the damping to fall off is shown by the results for the highest mean incidence (5°) and lowest frequency (36 c/s) in Fig. 11, but the drop is small compared with that obtained with Wing A. The effect of increasing mean incidence is to lower the level of the curves, mainly in going from $\alpha = 0°$ to $\alpha = 3°$. Increase of frequency tends on the whole to raise the level of the curves, but the effect is small except at 5° mean incidence.

Interpretation of the difference in the damping characteristics for the two models is difficult, since the tests were *ad hoc* in nature, the models being unrelated. If, however, apex angle is regarded as the important parameter, the results appear to substantiate free-flight missile tests[4] made in the U.S.A., which indicated that a delta wing with 60° apex angle is free from loss of pitching damping in the transonic range of speed. Other American tests[5] have shown that with a 90° apex angle loss of damping occurs. These results are also indicated by the theoretical work of Mangler[6].

The stiffness derivative $(-m_{\theta})$ curves for Wing A at 0° mean incidence exhibit a dip commencing at $M = 0{\cdot}9$. This corresponds to a forward movement of the aerodynamic centre observed during static tests made at the R.A.E.[7]. The absence of a dip in the curves for $\alpha = 3°$ and 5° is also in agreement with these tests, since no forward movement of the aerodynamic centre was observed at these incidences. The shape of the stiffness curves for Wing B suggests a comparatively smoother movement of the aerodynamic centre.

The reality of the amplitude effect in the results for Wing B is difficult to assess, since the earlier subsonic tests[2] showed that this planform is particularly sensitive to tunnel flow conditions. However, the general shape of the curves is unaltered by change of amplitude. The tests on Wing A were limited to one amplitude of oscillation, since the earlier tests with solid liners had shown no appreciable amplitude effect.

4.2. *Wing $\bar{A}$ (without body).*

Curves relating $-m_{\dot{\theta}}$ and $-m_{\theta}$ to M for the model without body are given in Figs. 13 and 14

and with body in Figs. 15 and 16. The curves in Figs. 13 and 14 showing the variation of ω with M apply to both mean incidences and the tests with body to within $\frac{1}{2}\%$.

For the case without the body the damping derivative $-m_{\dot{\theta}}$ increases to a maximum in the neighbourhood of $M = 0{\cdot}95$, the maximum value being approximately 100% greater than the value at $M = 0{\cdot}7$. Above $M = 0{\cdot}95$ a rapid falling-off occurs, which in the case of the test at incidence with the lower frequency leads to zero damping at approximately $M = 1{\cdot}07$. The effect of increasing frequency is to reduce the rate of loss of damping in the test at incidence.

The stiffness derivatives $-m_{\theta}$ shows little variation with Mach number up to $M = 1{\cdot}0$, after which a rapid increase occurs consistent with rearward movement of the aerodynamic centre (*see* Section 5). Below $M = 1$ the stiffness derivative is greater with the model at incidence.

Corresponding curves for Wing A ($0{\cdot}556\ c_0$ axis) are included in Figs. 13 and 14 for comparison, since the two wings have somewhat similar planforms. The variation of $-m_{\dot{\theta}}$ with Mach number is similar, but in the case of the tests at incidence on Wing A the maximum occurs somewhat earlier and the fall in damping leads to negative values. As for Wing $\bar{A}$ increase of frequency reduces the rate of loss of damping in the test at incidence. The curves of $-m_{\theta}$ against M for Wing A at 0° mean incidence show a pronounced dip commencing at approximately $M = 0{\cdot}9$, which corresponds to a rapid forward movement of the aerodynamic centre observed in R.A.E. static tests[3]. This effect is present only to a very small extent in the corresponding curves for Wing $\bar{A}$.

4.3. *Wing $\bar{A}$ (with body).*

The effect of the body on $-m_{\dot{\theta}}$ in the tests on Wing $\bar{A}$ is to reduce the increase at $M = 0{\cdot}95$ by 40 to 50% and to steepen the falling part of the curve. At $M = 1{\cdot}0$, however, the curve now ceased to fall and begins to rise sharply. The curves of $-m_{\theta}$ show a small dip at approximately $M = 0{\cdot}97$. Curves of $-m_{\theta}$ derived from static tests (unpublished) made at the R.A.E. for the case with body are included for comparison. These results are discussed in Section 5.

It is difficult to draw reliable conclusions from these tests since the body is largely immersed in the tunnel wall boundary layer*. The results are of value, however, in showing that the presence of a body may have an important and probably beneficial effect on the damping in the transonic regime.

It is interesting to observe that the influence of the body is negligible at the lowest Mach number of the range ($M = 0{\cdot}7$), a result which is in agreement with low-speed tests[8] made by G. F. Moss at the R.A.E. using complete models situated in the centre of the tunnel working section.

4.4. *Wing C.*

Curves relating $-m_{\dot{\theta}}$, $-m_{\theta}$ and ω to M are given in Figs. 17 and 18. The ω values apply to both mean incidences to within 1%.

Broadly speaking the curves of $-m_{\dot{\theta}}$ against M are similar to those for Wings $\bar{A}$ and A, the resemblance being closest to the latter. The maxima occur at approximately $M = 0{\cdot}93$ for $\alpha = 0°$ and somewhat earlier at $M = 0{\cdot}90$ for $\alpha = 3°$, whilst the falling part of the curve leads to negative damping in the test at incidence at the lower frequency. The shape of the curves near the highest Mach number of the tests suggests that the damping will increase as M is raised still more. Increase of frequency has little effect on the rate of loss of damping in this case, but raises the curves bodily.

---

* Measurements made with solid liners fitted to the tunnel indicated that the drop in ρV^2 was approximately 7% and 25% at 0·5 in. and 0·25 in. from the tunnel wall respectively.

At the lower Mach numbers the stiffness derivative $-m_\theta$ shows little variation with M, but above $M = 0{\cdot}9$ large changes occur, the curve for $\alpha = 0°$ developing a pronounced dip and that for $\alpha = 3°$ a peak. This results in large changes of $-m_\theta$ with incidence in the neighbourhood of $M = 1{\cdot}0$ which are of opposite sign to the changes observed below $M = 0{\cdot}9$.

Curves of $-m_{\dot\theta}$ and $-m_\theta$ obtained with solid liners[2] are included for comparison. The differences are attributed to altered blockage effects and tunnel wall interference as in the case of Wings A and B.

5. *Effect of Aerodynamic-Centre Movement.*

Values of $-m_\theta$ for very low frequencies and small amplitudes of oscillation can be obtained from static measurements of C_L and C_M, the relation being

$$-m_\theta = \tfrac{1}{2}\frac{\partial C_L}{\partial \theta} \times \left(-\frac{\partial C_M}{\partial C_L}\right).$$

The factor $-\partial C_M/\partial C_L$ is equal to the distance of the aerodynamic centre (A.C.) behind the axis expressed as a fraction of the mean chord, and in the present case is a small quantity. Thus, provided $\partial C_L/\partial\theta$ remains sensibly constant, small movements of the A.C. with Mach number will have an appreciable effect on $-m_\theta$, an increase corresponding to a rearward movement and a decrease to a forward movement of the A.C.

For larger amplitudes of oscillation of the order of those employed in the present tests, considerable movement of the A.C. takes place during the oscillation at the higher Mach numbers due to the changes in incidence. The pitching moment for this condition is a non-linear function of angular displacement and the correspondence between $-m_\theta$ and the A.C. position at the mean incidence becomes approximate only. The precise meaning to be given to the experimentally determined $-m_\theta$ when the pitching moment is non-linear is discussed in the Appendix.

In the case of the tests on Wing C, the axis is so close to the average aerodynamic-centre position that large non-linearities occur. The displacement is somewhat greater for Wing Ā and since the R.A.E. static tests referred to in Section 4.3 indicate that little movement of the aerodynamic centre with change of incidence occurs up to 3° at Mach numbers ranging up to 0·87, zero-frequency values of $-m_\theta$ have been derived from them and plotted in Figs. 15 and 16 for comparison with the oscillatory results. Even in this case the A.C. is only approximately $0{\cdot}1\bar{c}$ behind the axis, and small displacements due to the influence of tunnel walls or the model boundary-layer condition are likely to have large effects on $-m_\theta$. This probably explains the difference between the static and oscillatory results.

6. *Comparison with Theory.*

A theoretical curve for subsonic values of $-m_{\dot\theta}$ calculated by Garner[9] for Wing A, on the basis of Multhopp's theory is included in Fig. 7. These results were obtained by satisfying the downwash condition at seven spanwise and two chordwise positions, and they apply to infinitesimally small values of the frequency parameter.

A value of $-m_{\dot\theta}$ for $M = 1$ calculated by Mangler[6] is plotted in both Fig. 7 and Fig. 8. These results relate to the values of ω for $M = 1$ on the experimental curves, and they show the same trends with frequency as given by experiment, i.e. $-m_{\dot\theta}$ increases with increasing ω. In Fig. 7 the results due to Garner and Mangler taken together suggest a peak (shown dotted) at approximately the same Mach number as the peak on the experimental curve.

Two theoretical subsonic values of $-m_\theta$ calculated by Garner[9] are included in Fig. 7. These results are derived from steady motion theory, the downwash condition being satisfied at the same points as for $-m_{\dot{\theta}}$.

No theoretical values for the other planforms are available.

7. *Comparisons with American Results.*

Measurements of $-m_{\dot{\theta}}$ for a delta with a 90° apex angle have been made by Tobak, Reese and Beam[5] at subsonic and supersonic speeds. The only results for an axis position close to that of the N.P.L. tests on Wing A relate to an uncropped delta with body ($0{\cdot}567c_0$ axis, NACA 006–63 section), and a comparison is made in Fig. 19. For completeness the theoretical results of Garner and Mangler are included, together with a theoretical curve for supersonic speeds due to Acum[10] based on linearized lifting-surface theory.

It is difficult to make a satisfactory comparison of the experimental results on account of the unknown effect of the body in the American tests. A possible explanation of the comparative delay in the loss of damping in the N.P.L. tests, however, may be sought in the stabilizing effect of the cropped tips. Some effect might also be expected from the difference in thickness-chord ratio, which was 6% in the American tests as compared with 10% for Wing A, but if measurements of lift coefficient are taken as a guide the thinner section would be expected to show the delay.

8. *Conclusions.*

8.1. *Wing A.*

(i) With increasing Mach number the damping rises to a maximum in the neighbourhood of $M = 0{\cdot}95$. This is followed by a rapid fall.

(ii) The maximum damping occurs at a smaller Mach number in the tests at 3° and 5° mean incidence than at 0°, and has a considerably greater value at 5°.

(iii) In the tests at incidence the fall in damping leads to negative values at the lower frequency. A return to positive values at higher values of M is indicated.

(iv) The rate of fall in damping is reduced by increase of frequency in the tests at incidence (slotted liner tests).

(v) The stiffness curves for 0° mean incidence indicate a rapid forward movement of the aerodynamic centre commencing at $M = 0{\cdot}9$ (slotted-liner tests).

8.2. *Wing B.*

(i) The damping varies comparatively little over the whole Mach number range, relatively small fluctuations occurring at the upper end. A small loss of damping occurs only at the highest mean incidence (5°) with the lowest frequency.

(ii) Increase in mean incidence lowers the level of the damping curves, mainly in going from 0° to 3°.

(iii) Increase of frequency tends to raise the level of the curves.

(iv) The stiffness curves indicate a comparatively smooth movement of the aerodynamic centre.

8.3. *Wing $\bar{A}$ (without Body).*

(i) With increase of Mach number from $0{\cdot}7$ to $0{\cdot}95$ the damping increases by approximately 100% to a maximum value which is followed by a rapid fall.

(ii) In the tests at incidence (3°) the fall in damping leads to zero damping at approximately $M = 1 \cdot 07$ at the lower frequency.

(iii) The rate of fall in damping in the tests at incidence is reduced by increase of frequency.

(iv) The stiffness shows little variation with Mach number up to $M = 1 \cdot 0$. Above this value a rapid increase occurs.

8.4. *Wing $\bar{A}$ (with Body).*

(i) The rise in damping with Mach number is now reduced to about 50% of its value at $M = 0 \cdot 7$. The damping at this Mach number is substantially the same as without the body.

(ii) The falling part of the curve is steepened, but now ceases to fall at $M = 1 \cdot 0$ and begins to rise sharply.

(iii) The effect of the body on the stiffness curves is small.

8.5. *Wing C.*

(i) A variation of damping with Mach number similar to that for Wing $\bar{A}$ without body is obtained, the rise in damping being somewhat less and the maxima occurring earlier at $M = 0 \cdot 93$ for 0° incidence and $M = 0 \cdot 90$ for 3° incidence.

(ii) In the tests at incidence (3°) the fall in damping leads to negative values above $M = 1 \cdot 02$ at the lower frequency.

(iii) Increase in frequency raises the curves bodily.

(iv) Large changes of stiffness with mean incidence are observed in the neighbourhood of $M = 1 \cdot 0$ which are of opposite sign to those obtained below $M = 0 \cdot 9$.

Comparison of the results for Wings A and B lends support to the indications of theory and of American tests to the effect that a delta with 60° apex angle is stable in the transonic regime, whilst with 90° apex angle instability may arise.

NOTATION

M'		Pitching moment
	$=$	$M_\theta\theta + M_{\dot\theta}\dot\theta$
θ		Angular displacement
θ_0		Amplitude of oscillation
α		Mean incidence
m_θ	$=$	$M_\theta/\rho SV^2\bar{c}$
$m_{\dot\theta}$	$=$	$M_{\dot\theta}/\rho SV\bar{c}^2$
ρ		Density
S		Area
V		Wind speed
$\bar{c}$		Mean chord
c_0		Root chord
f		Frequency (in wind)
f_0		Frequency (in still air)

REFERENCES

No.	*Author(s)*	*Title, etc.*
1	J. B. Bratt, W. G. Raymer and J. E. G. Townsend.	Measurements of the direct pitching-moment derivatives for two-dimensional flow at subsonic and supersonic speeds and for a wing of aspect ratio 4 at subsonic speeds. A.R.C. R. & M. 3257. January, 1959.
2	J. B. Bratt, W. G. Raymer and J. E. G. Townsend.	Measurements of the direct pitching-moment derivatives for three wing planforms at high subsonic speeds. A.R.C. R. & M. 3419. November, 1953.
3	D. W. Holder, R. J. North and A. Chinneck.	Experiments with slotted and perforated walls in a two-dimensional high-speed tunnel. A.R.C. R. & M. 2955. November, 1951.
4	G. L. Mitcham, J. E. Stevens and H. P. Norris.	Aerodynamic characteristics and flying qualities of a tailless triangular-wing airplane configuration as obtained from flights of rocket-propelled models at transonic and low supersonic speeds. N.A.C.A. Tech. Note 3753. November, 1956.
5	M. Tobak, D. E. Reese and B. H. Beam.	Experimental damping in pitch of 45° triangular wings. N.A.C.A. Research Memo. A50J26 (TIB/2725). December, 1950.
6	K. W. Mangler	A method of calculating the short period longitudinal stability derivatives of a wing in linearized unsteady compressible flow. R.A.E. Report Aero. 2468. A.R.C. 15 316. June, 1952.
7	J. Y. G. Evans and M. Jones ..	High speed tunnel tests on a 1/12.2 scale model of a delta-winged aircraft (Boulton Paul E.27/46). R.A.E. Report Aero. 2328. A.R.C. 12 908. August, 1949.
8	G. F. Moss	Low-speed wind tunnel measurements of longitudinal oscillatory derivatives on three wing planforms. A.R.C. R. & M. 3009. November, 1952.
9	H. C. Garner	Multhopp's subsonic lifting surface theory of wings in slow pitching oscillations. A.R.C. R. & M. 2885. July, 1952.
10	W. E. A. Acum	Aerodynamic forces on cropped delta wings performing pitching oscillations in a supersonic stream. To be published.

APPENDIX

Measurements with Non-linear Aerodynamic Stiffness.

In the self-excitation technique employed in the present tests the damping forces are automatically balanced by an electrical drive to give a sustained oscillation. The damping derivative $m_{\dot\theta}$ is then derived from measurements of power input and the stiffness derivative m_θ from the change in period of the motion produced by the wind loading. The value of m_θ is calculated on the assumption that the aerodynamic moment is proportional to angular displacement.

If the aerodynamic moment is a non-linear function of displacement, the equation of motion may be written in the form

$$I\ddot\theta + \{\sigma + F(\theta)\}\theta = 0\,, \tag{1}$$

when I is moment of inertia, σ is elastic stiffness, and $F(\theta)$ the aerodynamic stiffness coefficient which is now a function of displacement θ.

Equation (1) leads to

$$\frac{dt}{d\theta} = I^{1/2}\left\{\sigma(\theta_1^2-\theta^2) + 2\int_\theta^{\theta_1}\theta F(\theta)d\theta\right\}^{-1/2}, \tag{2}$$

and

$$\sigma(\theta_1^2-\theta_2^2) + 2\int_{-\theta_2}^{\theta_1}\theta F(\theta)d\theta = 0, \tag{3}$$

where θ_1 and θ_2 are the maximum positive and negative displacements respectively of the system from its equilibrium position.

In an experimental arrangement of the type under consideration elastic stiffness reactions are large compared with aerodynamic, the motion being closely simple harmonic. Thus (2) may be expanded and integrated to give the periodic time τ in the form

$$\begin{aligned}\tfrac{1}{2}\tau I^{-1/2} &= \sigma^{-1/2}\{\mathscr{I}_0(\theta_1) + \mathscr{I}_1(\theta_1)\sigma^{-1} + \mathscr{I}_2(\theta_1)\sigma^{-2} + \ldots\}\\ &\quad + \sigma^{-1/2}\{\mathscr{I}_0(\theta_2) + \mathscr{I}_1(\theta_2)\sigma^{-1} + \mathscr{I}_2(\theta_2)\sigma^{-2} + \ldots\},\end{aligned} \tag{4}$$

where

$$\mathscr{I}_0(\theta_1) = \int_0^{\theta_1}(\theta_1^2-\theta^2)^{-1/2}\,d\theta = \frac{\pi}{2}$$

$$\mathscr{I}_0(\theta_2) = \int_0^{\theta_2}(\theta_2^2-\theta^2)^{-1/2}\,d\theta = \frac{\pi}{2}$$

$$\mathscr{I}_1(\theta_1) = -\int_0^{\theta_1}\left\{\int_\theta^{\theta_1}\theta F(\theta)\,d\theta\right\}(\theta_1^2-\theta^2)^{-3/2}\,d\theta$$

$$\mathscr{I}_1(\theta_2) = -\int_0^{\theta_2}\left\{\int_\theta^{\theta_2}\theta F(-\theta)\,d\theta\right\}(\theta_2^2-\theta^2)^{-3/2}\,d\theta$$

$$\mathscr{I}_2(\theta_1) = \frac{3}{4}\int_0^{\theta_1}\left\{\int_\theta^{\theta_1}\theta F(\theta)d\theta\right\}^2(\theta_1^2-\theta^2)^{-5/2}\,d\theta$$

$$\mathscr{I}_2(\theta_2) = \frac{3}{4}\int_0^{\theta_2}\left\{\int_\theta^{\theta_2}\theta F(-\theta)d\theta\right\}^2(\theta_2^2-\theta^2)^{-5/2}\,d\theta$$

etc., ...

In still air the period τ_0 is given by

$$\tfrac{1}{2}\tau_0 I^{-1/2} = \sigma^{-1/2}\{\mathscr{I}_0(\theta_1) + \mathscr{I}_0(\theta_2)\} = \pi\sigma^{-1/2}, \tag{5}$$

and the change in period $\delta\tau$ due to the aerodynamic loading is obtained from (4) and (5) in the form

$$\tfrac{1}{2}\delta\tau I^{-1/2} = \sigma^{-3/2}[\mathscr{I}_1(\theta_1) + \mathscr{I}_1(\theta_2) + \sigma^{-1}\{\mathscr{I}_2(\theta_1) + \mathscr{I}_2(\theta_2)\} + \ldots]. \tag{6}$$

For small changes in period the stiffness derivative $-M_\theta$ is obtained from the relation

$$-M_\theta = -2\sigma\frac{\delta\tau}{\tau_0}, \tag{7}$$

which is derived on the assumption that the aerodynamic reaction varies linearly with displacement. Use of the same formula for the non-linear case leads to

$$-M_\theta = \frac{2}{\pi}[\mathscr{I}_1(\theta_1) + \mathscr{I}_1(\theta_2) + \sigma^{-1}\{\mathscr{I}_2(\theta_1) + \mathscr{I}_2(\theta_2)\} + \ldots]. \tag{8}$$

When σ is large terms involving negative powers of σ may be neglected, and from (3) it follows that θ_1 may be taken as equal to θ_2. Thus, when aerodynamic reactions are small compared with elastic reactions, equation (8) becomes

$$-M_\theta = \frac{2}{\pi}\int_\theta^{\theta_0} \frac{\int_\theta^{\theta_0} \theta\{F(\theta) + F(-\theta)\}\,d\theta}{\{\theta_0^2 - \theta^2\}^{3/2}}\,d\theta, \tag{9}$$

θ_0 being the amplitude of oscillation.

It is clear from the above result that the technique of measurement employed gives for each amplitude of oscillation an equivalent linear aerodynamic stiffness which, with a system having high elastic stiffness, produces the same frequency change as the actual non-linear stiffness.

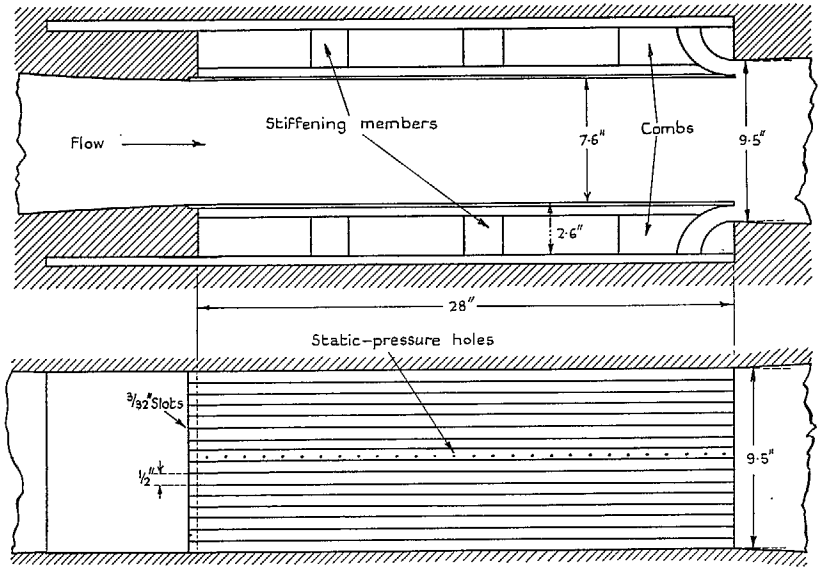

FIG. 1. Slotted liners.

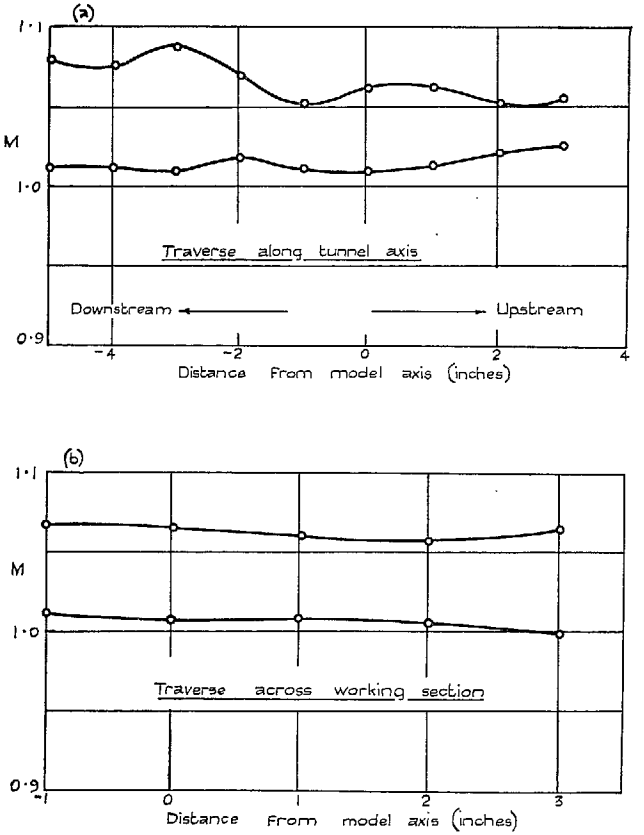

FIG. 2. Variation of M in working section.

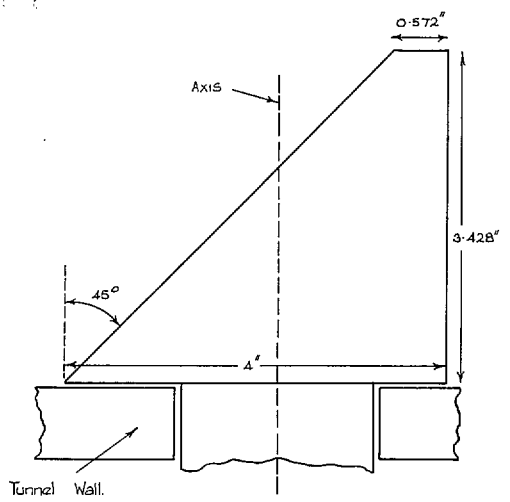

FIG. 3. Diagram of Wing A (half-scale).

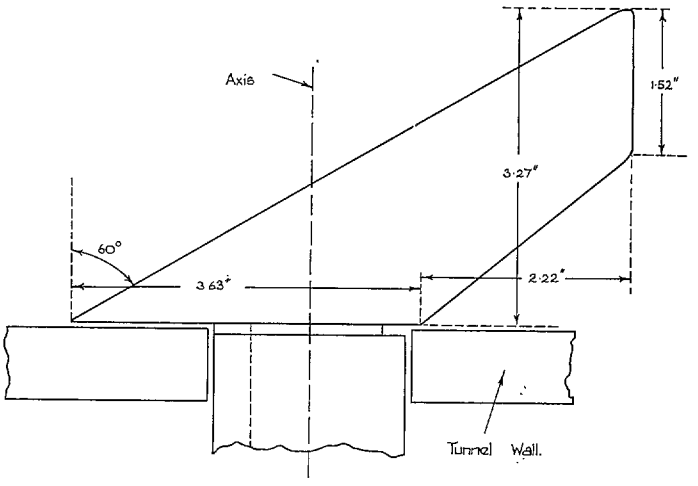

FIG. 4. Diagram of Wing B (half-scale).

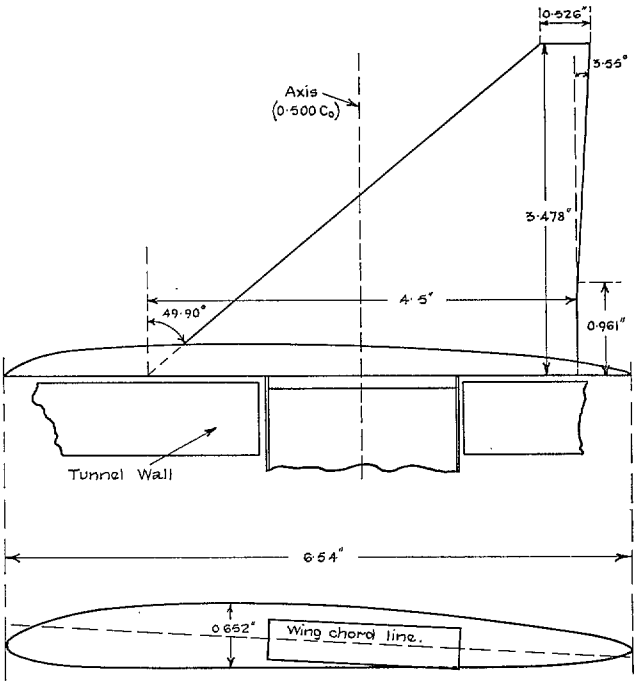

FIG. 5. Diagram of Wing $\bar{A}$ with body (half-scale).

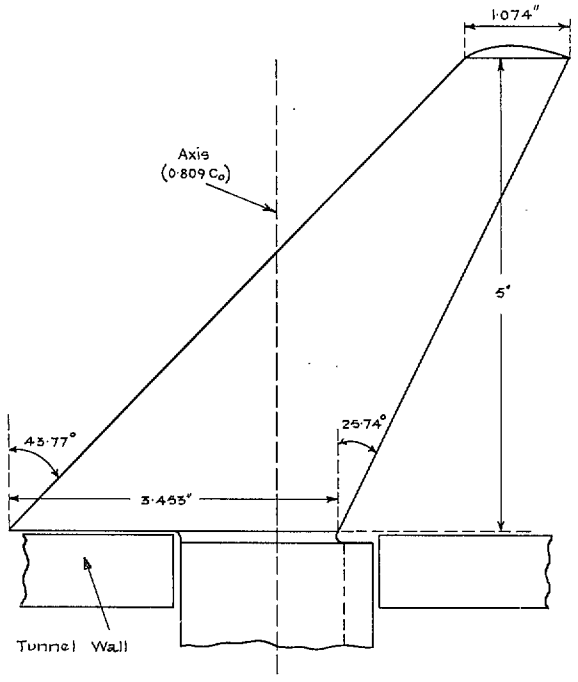

FIG. 6. Diagram of Wing C (half-scale).

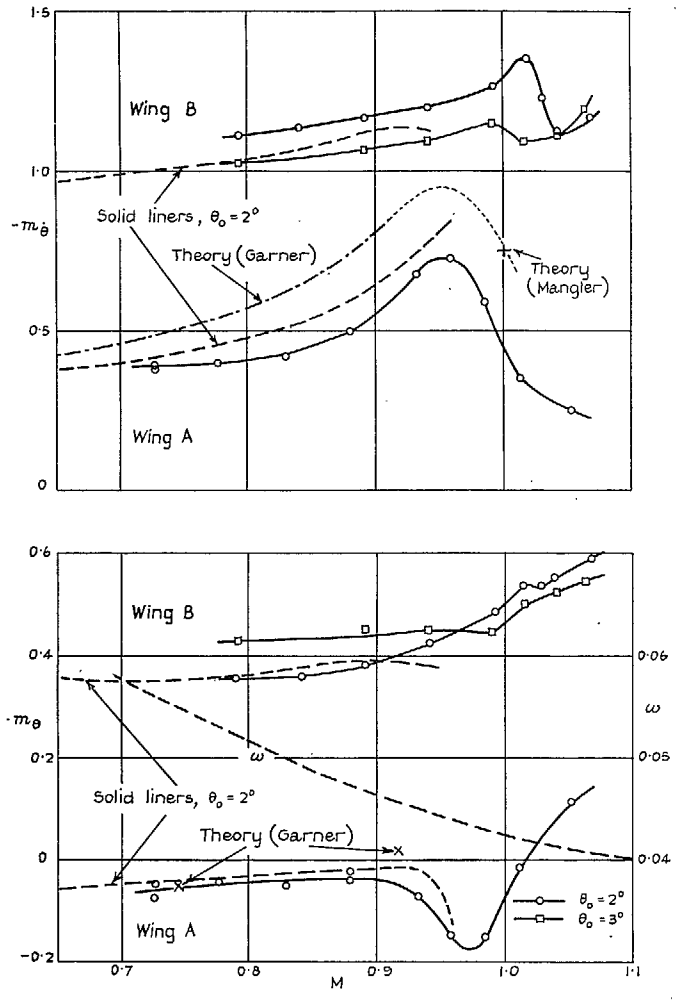

FIG. 7. Values of $-m_{\dot\theta}$ and $-m_\theta$ for wings A and B at $\alpha = 0°$ and $f_0 = 36$ c/s nominal.

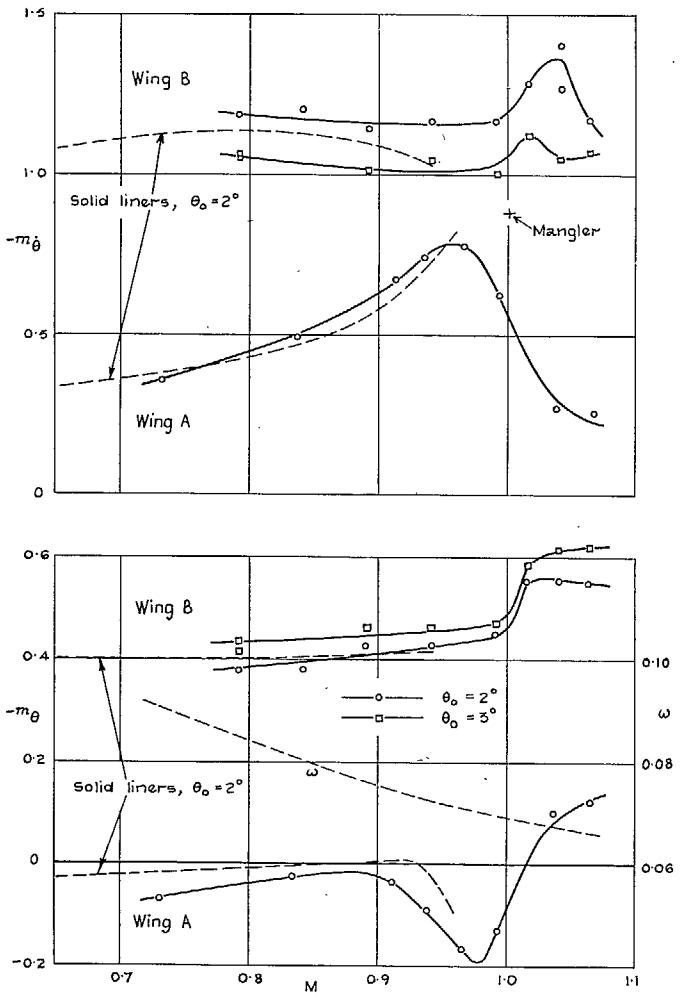

FIG. 8. Values of $-m_{\dot\theta}$ and $-m_\theta$ for wings A and B at $\alpha = 0°$ and $f_0 = 57$ c/s nominal.

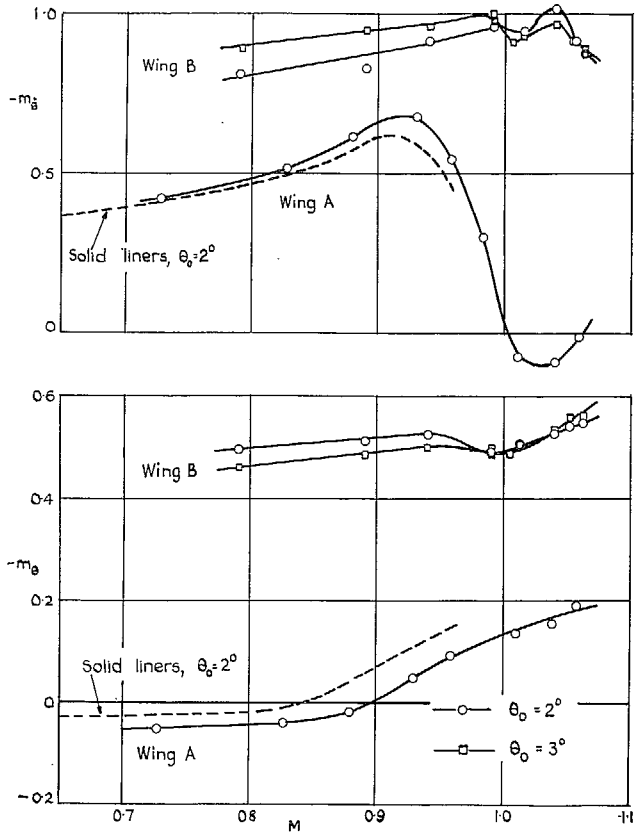

FIG. 9. Values of $-m_{\dot{\theta}}$ and $-m_\theta$ for wings A and B at $\alpha = 3°$ and $f_0 = 36$ c/s nominal.

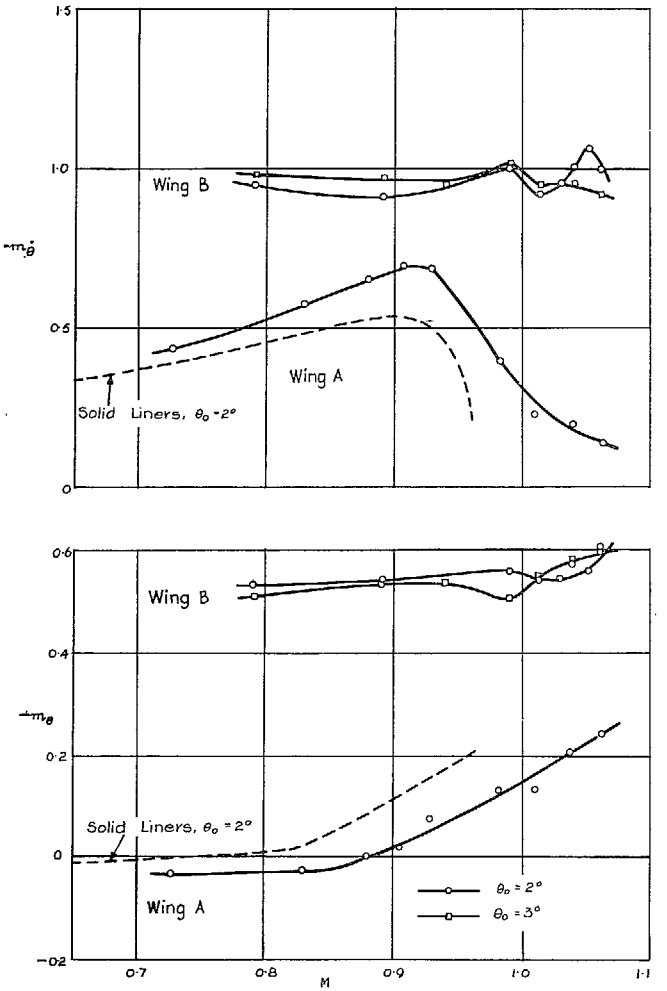

FIG. 10. Values of $-m_{\dot{\theta}}$ and $-m_\theta$ for wings A and B at $\alpha = 3°$ and $f_0 = 57$ c/s nominal.

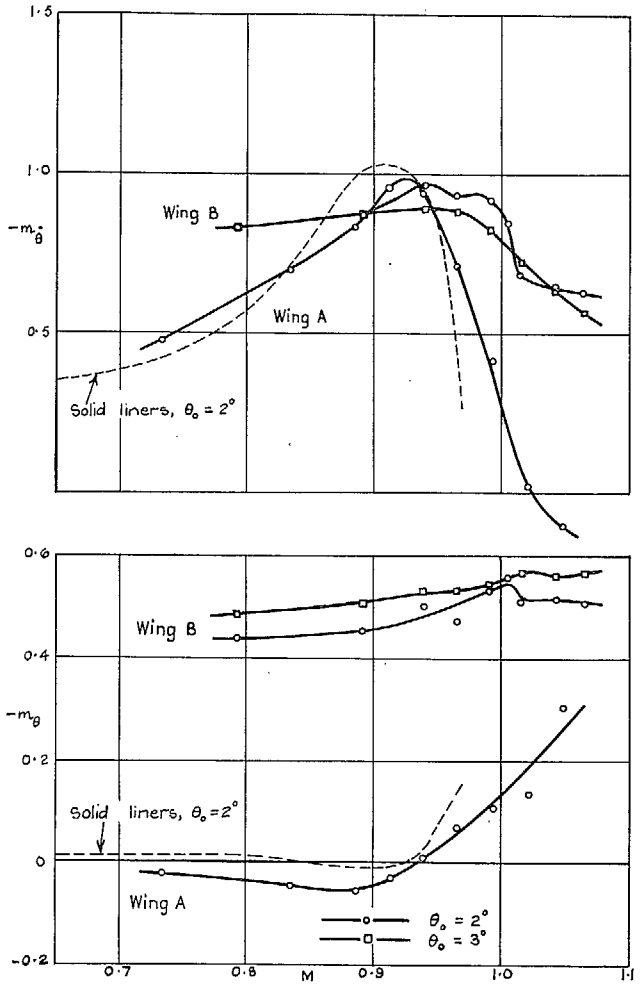

FIG. 11. Values of $-m_{\dot{\theta}}$ and $-m_\theta$ for wings A and B at $\alpha = 5°$ and $f_0 = 36$ c/s nominal.

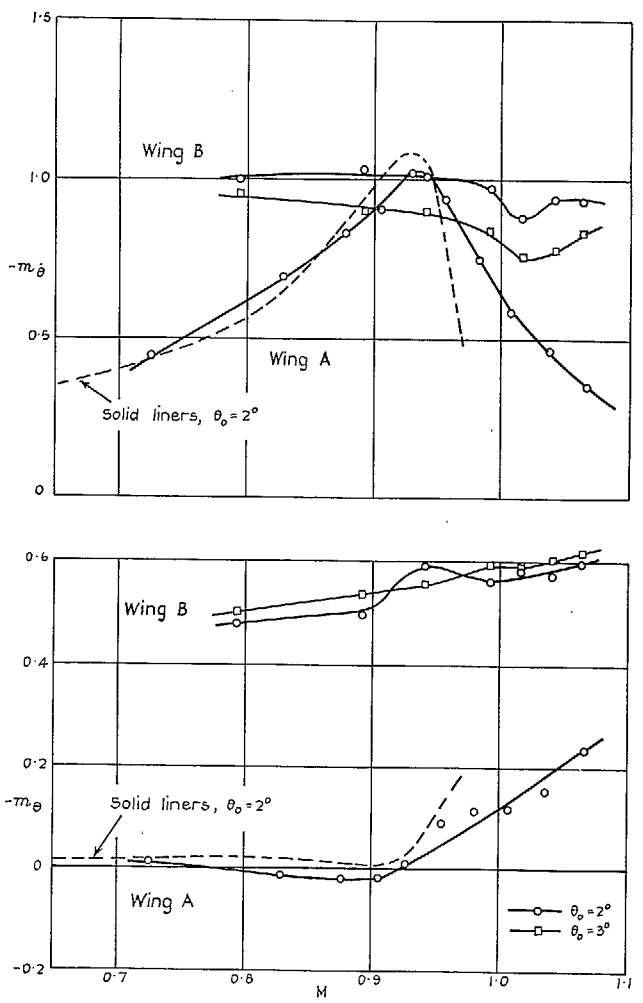

FIG. 12. Values of $-m_{\dot{\theta}}$ and $-m_\theta$ for wings A and B at $\alpha = 5°$ and $f_0 = 57$ c/s nominal.

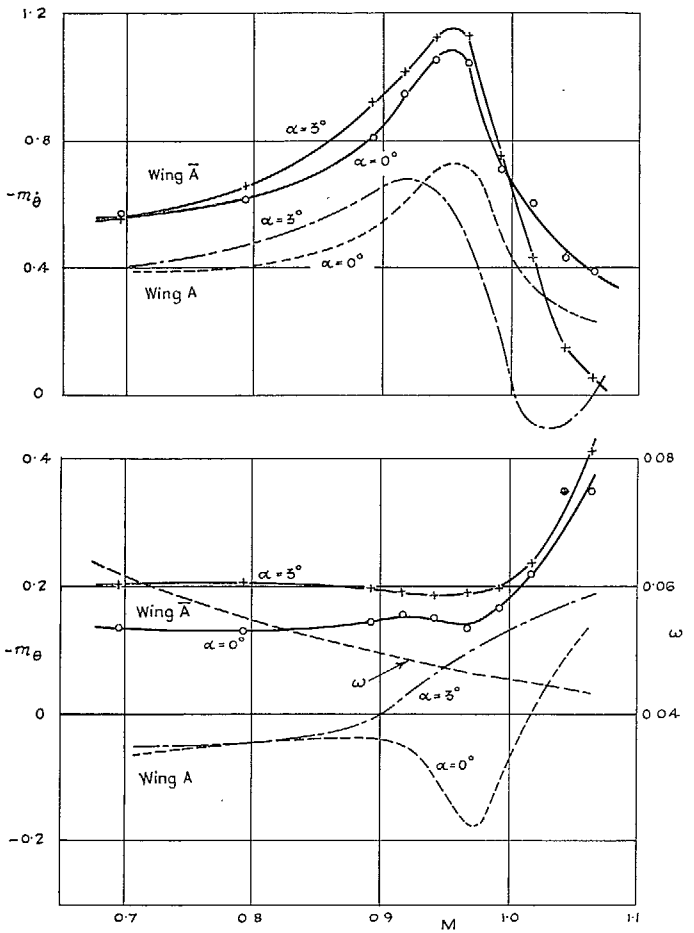

FIG. 13. Values of $-m_{\dot{\theta}}$ and $-m_{\theta}$ for wing $\bar{A}$ at $f_0 = 35$ c/s nominal.

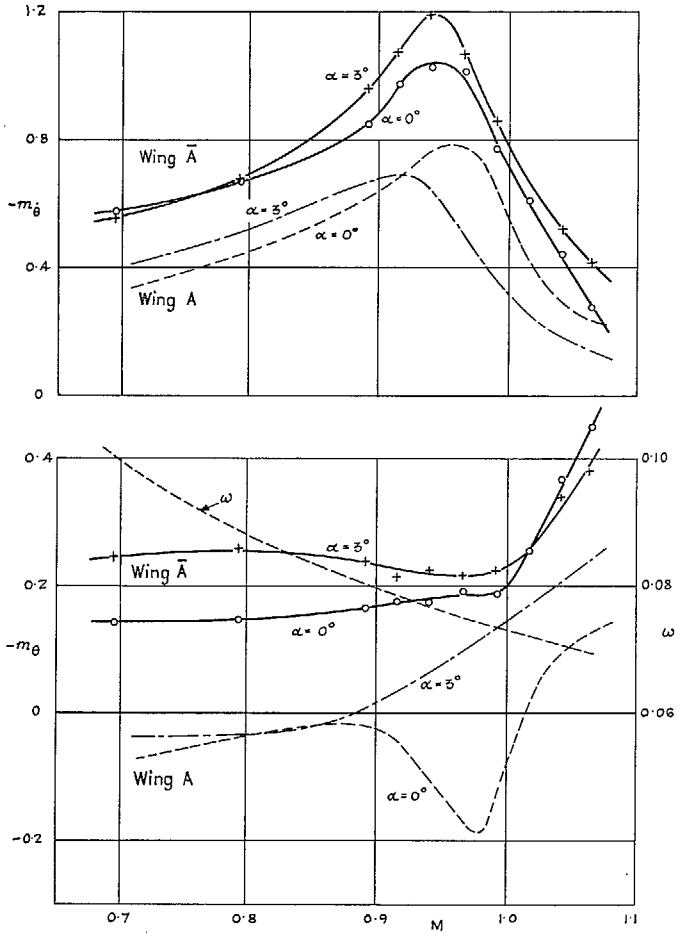

FIG. 14. Values of $-m_{\dot{\theta}}$ and $-m_{\theta}$ for wing $\bar{A}$ at $f_0 = 57$ c/s nominal.

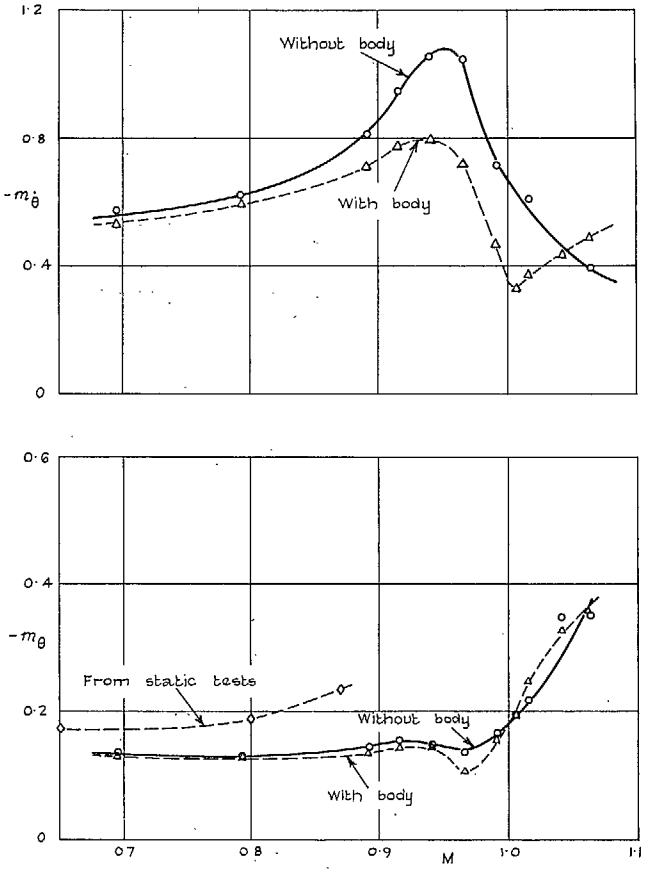

FIG. 15. Effect of body on wing $\overline{A}$ for $\alpha = 0°$ and $f_0 = 35$ c/s nominal.

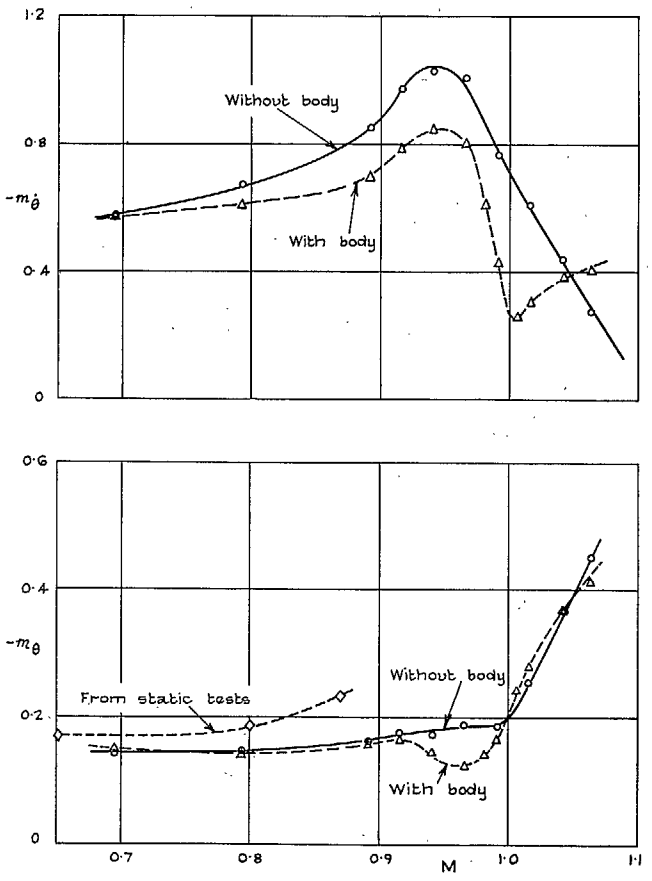

FIG. 16. Effect of body on wing $\overline{A}$ for $\alpha = 0°$ and $f_0 = 57$ c/s nominal.

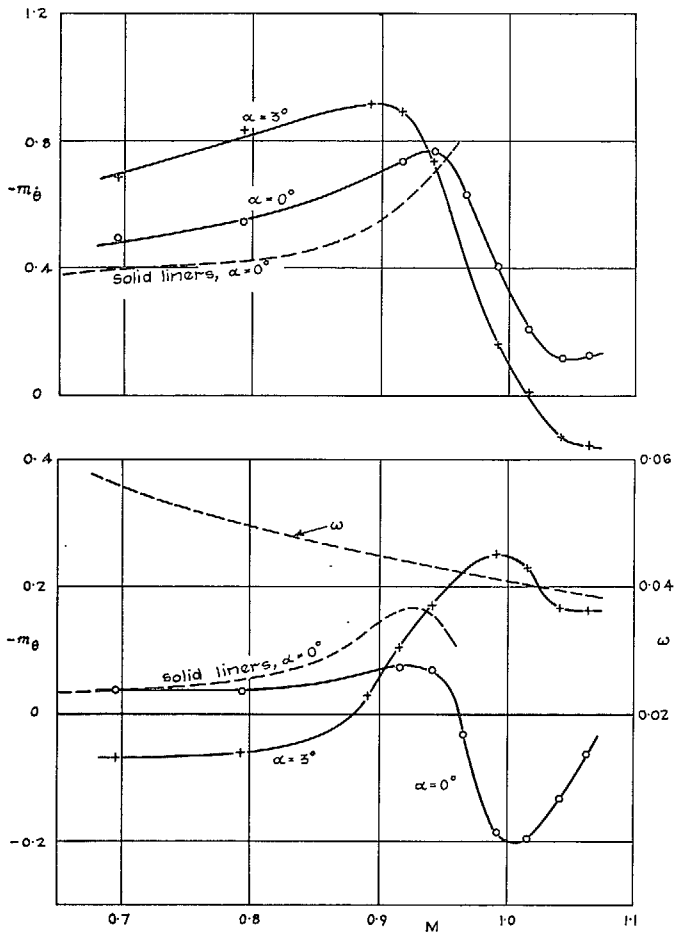

FIG. 17. Values of $-m_{\dot\theta}$ and $-m_\theta$ for wing C at $f_0 = 35$ c/s nominal.

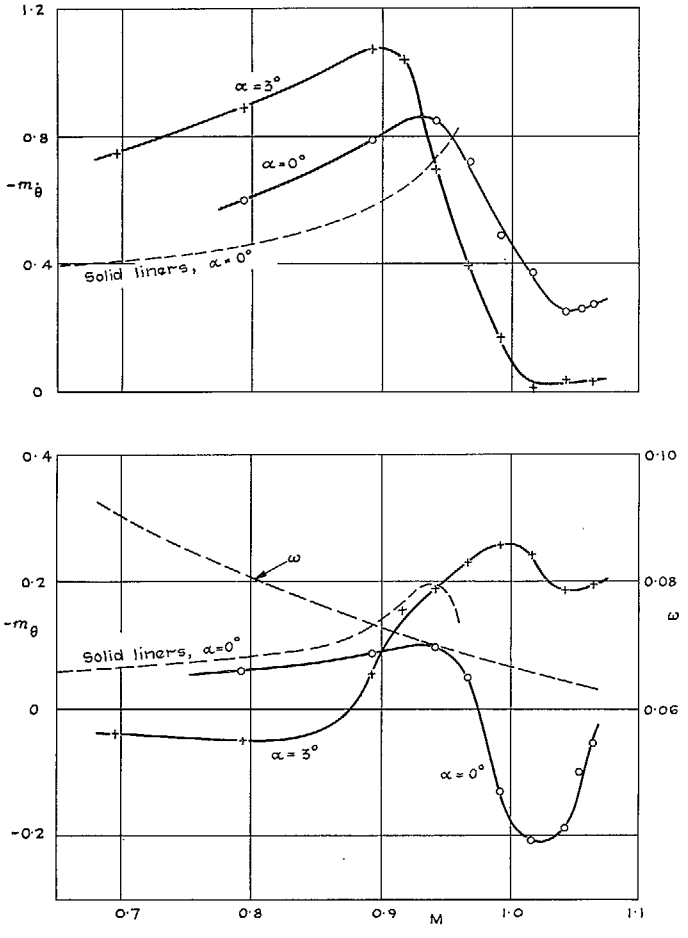

FIG. 18. Values of $-m_{\dot\theta}$ and $-m_\theta$ for wing C at $f_0 = 57$ c/s nominal.

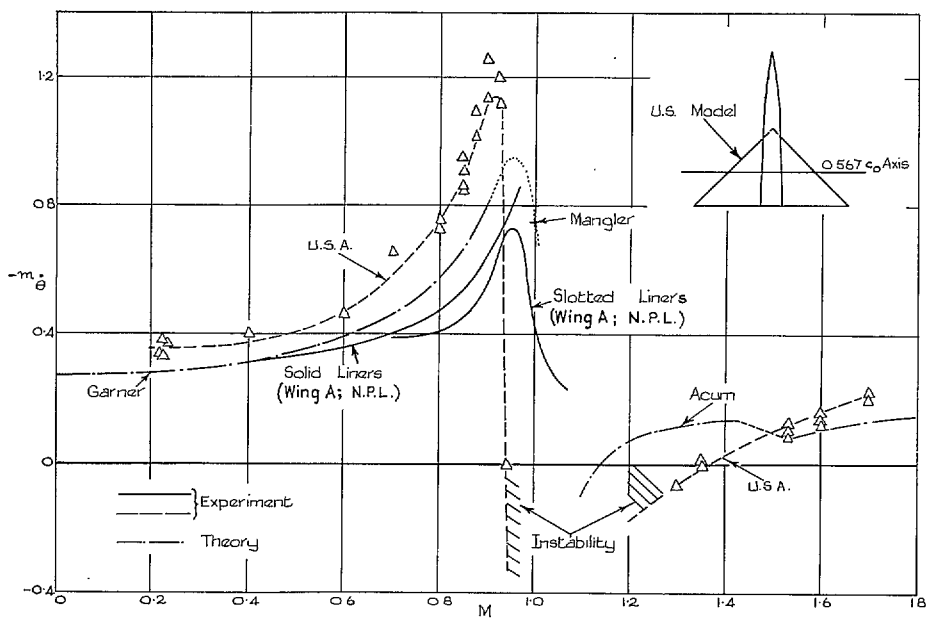

FIG. 19. Comparisons with American results.

(92795) Wt. 67/7689 K5 10/66 Hw.

Publications of the Aeronautical Research Council

ANNUAL TECHNICAL REPORTS OF THE AERONAUTICAL RESEARCH COUNCIL (BOUND VOLUMES)

1945 Vol. I. Aero and Hydrodynamics, Aerofoils. £6 10*s*. (£6 14*s*.)
Vol. II. Aircraft, Airscrews, Controls. £6 10*s*. (£6 14*s*.)
Vol. III. Flutter and Vibration, Instruments, Miscellaneous, Parachutes, Plates and Panels, Propulsion. £6 10*s*. (£6 14*s*.)
Vol. IV. Stability, Structures, Wind Tunnels, Wind Tunnel Technique. £6 10*s*. (£6 14*s*.)

1946 Vol. I. Accidents, Aerodynamics, Aerofoils and Hydrofoils. £8 8*s*. (£8 12*s*. 6*d*.)
Vol. II. Airscrews, Cabin Cooling, Chemical Hazards, Controls, Flames, Flutter, Helicopters, Instruments and Instrumentation, Interference, Jets, Miscellaneous, Parachutes. £8 8*s*. (£8 12*s*.)
Vol. III. Performance, Propulsion, Seaplanes, Stability, Structures, Wind Tunnels. £8 8*s*. (£8 12*s*.)

1947 Vol. I. Aerodynamics, Aerofoils, Aircraft. £8 8*s*. (£8 12*s*. 6*d*.)
Vol. II. Airscrews and Rotors, Controls, Flutter, Materials, Miscellaneous, Parachutes, Propulsion, Seaplanes, Stability, Structures, Take-off and Landing. £8 8*s*. (£8 12*s*. 6*d*.)

1948 Vol. I. Aerodynamics, Aerofoils, Aircraft, Airscrews, Controls, Flutter and Vibration, Helicopters, Instruments, Propulsion, Seaplane, Stability, Structures, Wind Tunnels. £6 10*s*. (£6 14*s*.)
Vol. II. Aerodynamics, Aerofoils, Aircraft, Airscrews, Controls, Flutter and Vibration, Helicopters, Instruments, Propulsion, Seaplane, Stability, Structures, Wind Tunnels. £5 10*s*. (£5 14*s*.)

1949 Vol. I. Aerodynamics, Aerofoils. £5 10*s*. (£5 14*s*.)
Vol. II. Aircraft, Controls, Flutter and Vibration, Helicopters, Instruments, Materials, Seaplanes, Structures, Wind Tunnels. £5 10*s*. (£5 13*s*. 6*d*.)

1950 Vol. I. Aerodynamics, Aerofoils, Aircraft. £5 12*s*. 6*d*. (£5 16*s*. 6*d*.)
Vol. II. Apparatus, Flutter and Vibration, Meteorology, Panels, Performance, Rotorcraft, Seaplanes. £4 (£4 3*s*. 6*d*.)
Vol. III. Stability and Control, Structures, Thermodynamics, Visual Aids, Wind Tunnels. £4 (£4 3*s*. 6*d*.)

1951 Vol. I. Aerodynamics, Aerofoils. £6 10*s*. (£6 14*s*.)
Vol. II. Compressors and Turbines, Flutter, Instruments, Mathematics, Ropes, Rotorcraft, Stability and Control, Structures, Wind Tunnels. £5 10*s*. (£5 14*s*.)

1952 Vol. I. Aerodynamics, Aerofoils. £8 8*s*. (£8 12*s*.)
Vol. II. Aircraft, Bodies, Compressors, Controls, Equipment, Flutter and Oscillation, Rotorcraft, Seaplanes, Structures. £5 10*s*. (£5 13*s*. 6*d*.)

1953 Vol. I. Aerodynamics, Aerofoils and Wings, Aircraft, Compressors and Turbines, Controls. £6 (£6 4*s*.)
Vol. II. Flutter and Oscillation, Gusts, Helicopters, Performance, Seaplanes, Stability, Structures, Thermodynamics, Turbulence. £5 5*s*. (£5 9*s*.)

1954 Aero and Hydrodynamics, Aerofoils, Arrester gear, Compressors and Turbines, Flutter, Materials, Performance, Rotorcraft, Stability and Control, Structures. £7 7*s*. (£7 11*s*.)

Special Volumes

Vol. I. Aero and Hydrodynamics, Aerofoils, Controls, Flutter, Kites, Parachutes, Performance, Propulsion, Stability. £6 6*s*. (£6 9*s*. 6*d*.)
Vol. II. Aero and Hydrodynamics, Aerofoils, Airscrews, Controls, Flutter, Materials, Miscellaneous, Parachutes, Propulsion, Stability, Structures. £7 7*s*. (£7 10*s*. 6*d*.)
Vol. III. Aero and Hydrodynamics, Aerofoils, Airscrews, Controls, Flutter, Kites, Miscellaneous, Parachutes, Propulsion, Seaplanes, Stability, Structures, Test Equipment. £9 9*s*. (£9 13*s*. 6*d*.)

Reviews of the Aeronautical Research Council

1949–54 5*s*. (5*s*. 6*d*.)

Index to all Reports and Memoranda published in the Annual Technical Reports

1909–1947 R. & M. 2600 (out of print)

Indexes to the Reports and Memoranda of the Aeronautical Research Council

Between Nos. 2451–2549: R. & M. No. 2550 2*s*. 6*d*. (2*s*. 9*d*.); Between Nos. 2651–2749: R. & M. No. 2750 2*s*. 6*d*. (2*s*. 9*d*.); Between Nos. 2751–2849: R. & M. No. 2850 2*s*. 6*d*. (2*s*. 9*d*.); Between Nos. 2851–2949: R. & M. No. 2950 3*s*. (3*s*. 3*d*.); Between Nos. 2951–3049: R. & M. No. 3050 3*s*. 6*d*. (3*s*. 9*d*.); Between Nos. 3051–3149: R. & M. No. 3150 3*s*. 6*d*. (3*s*. 9*d*.); Between Nos. 3151–3249: R. & M. No. 3250 3*s*. 6*d*. (3*s*. 9*d*.); Between Nos. 3251–3349: R. & M. No. 3350 3*s*. 6*d*. (3*s*. 11*d*.)

Prices in brackets include postage

Government publications can be purchased over the counter or by post from the Government Bookshops in London, Edinburgh, Cardiff, Belfast, Manchester, Birmingham and Bristol, or through any bookseller

Printed and published by
HER MAJESTY'S STATIONERY OFFICE

To be purchased from
49 High Holborn, London WC1
423 Oxford Street, London W1
13A Castle Street, Edinburgh 2
109 St. Mary Street, Cardiff
Brazennose Street, Manchester 2
50 Fairfax Street, Bristol 1
35 Smallbrook, Ringway, Birmingham 5
80 Chichester Street, Belfast 1
or through any bookseller

Printed in England

S.O. Code No. 23-3435